First principles analysis of the initial oxidation of Si(001) and Si(111) surfaces terminated with H and CH3

Huashan Li, Zhibin Lin, Zhigang Wu, and Mark T. Lusk

Related Articles

Multifunctional silicon inspired by a wing of male Papilio ulysse
Appl. Phys. Lett. 100, 033109 (2012)

Nonlinear behavior of photoluminescence from silicon particles under two-photon excitation
Appl. Phys. Lett. 99, 251105 (2011)

About the internal pressure in cavities derived from implantation-induced blistering in semi-conductors
J. Appl. Phys. 110, 114903 (2011)

Structural evolution of implanted vicinal Si(111) during annealing via analysis of the dipole contribution
J. Appl. Phys. 110, 103520 (2011)

Positive or negative gain: Role of thermal capture cross sections in impurity photovoltaic effect
J. Appl. Phys. 110, 104508 (2011)

Additional information on J. Chem. Phys.

First principles analysis of the initial oxidation of Si(001) and Si(111) surfaces terminated with H and CH₃

Huashan Li, Zhibin Lin, Zhigang Wu, and Mark T. Lusk[a)]
Department of Physics, Colorado School of Mines, 1523 Illinois Street, Golden, Colorado 80401, USA

Transition state analyses have been carried out within a density functional theory setting to explain and quantify the distinctly different ways in which hydrogen and methyl terminations serve to protect silicon surfaces from the earliest onset of oxidation. We find that oxidation occurs via direct dissociative adsorption, without any energy barrier, on Si(111) and reconstructed Si(001) that have been hydrogen terminated; oxidation initiates with a barrier of only 0.05 eV on unreconstructed Si(001). The commonly measured protection afforded by hydrogen is shown to derive from a coverage-dependent dissociation rate combined with barriers to the hopping of adsorbed oxygen atoms. Methyl termination, in contrast, offers an additional level of protection because oxygen must first undergo interactions with these ligands in a three-step process with significant energy barriers: adsorption of O_2 into a C–H bond to form a C–O–O–H intermediate; decomposition of C–O–O–H into C–O–H and C=O intermediates; and, finally, hopping of oxygen atoms from ligands to the substrate. © *2012 American Institute of Physics.* [doi:10.1063/1.3682782]

I. INTRODUCTION

The desire to understand, control, and exploit the oxidation of silicon (Si) has been a constant driving force in photovoltaics and micro-electronics research for over half a century. For example, precise control of the silicon/silicon oxide (Si/SiO₂) interface is required to embed extra-thin, high-dielectric material in metal-oxide semiconductor field effect transistors.[1] In solar cells composed of crystalline Si, post-oxidation effects result in defects such as dangling bonds at the SiO₂/Si interface which push the Fermi level towards the conduction band edge and increase the rate of electron-hole recombination,[2–4] thus deteriorating photo-conversion efficiency. The optical properties of Si nanostructures are particularly sensitive to oxidation because the high surface-to-volume ratio amplifies the effect of defects on electron-hole recombination. In addition, even slight oxidation of quantum confined nanostructures can have a striking influence on optical properties by changing the effective size of the remaining Si.[5]

The initial stage of oxidation on bare (unpassivated) Si surfaces has been investigated experimentally. Here oxygen atoms can directly attach to the exposed dangling bonds, and reflectance difference oscillation data suggests a layer-by-layer oxidation process that slows down with increasing oxide thickness.[6] Based on scanning reflection electron microscopy and Auger analysis, Watanabe *et al.*[7] argued that oxidation of the first layer of the bare Si(001) surface was barrierless and estimated an *effective* activation energy of 0.3 eV for second layer oxidation.

Surface passivation can profoundly reduce the rate of oxidation by blocking the dissociative adsorption of O₂ onto Si surface bonds. For instance, simple hydrogen (H) termination is widely used to protect against oxidation. At room temperature, both reconstructed Si–H and unreconstructed Si–H₂ Si(001) surfaces result from standard production techniques,[8] and these surfaces have been subjected to intense experimental scrutiny using scanning tunneling microscopy,[9] atomic force microscopy,[10, 11] x-ray photo electron spectroscopy,[12–15] Auger electron spectroscopy,[16] Fourier transform infrared spectroscopy (FTIR),[10, 17–22] and high-resolution electron energy-loss spectroscopy.[23–26] The FTIR spectrum exhibits a stable Si–H peak at early stages of oxidation[23, 25, 27] accompanied by an increasing Si(Oₓ)–H signal that grows slowly over time. This is consistent with the standard kinetic model for oxidation in which most O atoms are adsorbed into the Si–Si backbonds.

The rate of oxidation is strongly influenced by surface preparation and environment, but careful measurements of the formation of an oxide monolayer have been carried out as a function of temperature by Zhang *et al.*[28, 29] These were used to estimate *effective* (time averaged) activation energies for initial stage oxidation on H–Si(111), H–Si(001), and H₂–Si(001) surfaces as 1.7, 1.7, and 1.6 eV, respectively.[28, 29] For the sake of clarity in summarizing this work, we focus on H–Si(111).[29] Within a pure oxygen environment, oxidation was tracked by measuring the change of the FTIR peaks of Si–H and Si(Oₓ) at 573 K, 593 K, and 643 K. When fitted to a standard rate equation,

$$\frac{\partial [Si-H]}{\partial t} = k[Si-H]^{\alpha} P_{O_2}^{\beta}, \tag{1}$$

the reaction order, α, was estimated to be 1.5, suggesting a multistep oxidation process. The strong presence of H–SiO₂ and H–SiO₃ peaks in the spectrum led Zhang *et al.* to conclude that the multistep character derived from the influence of subsequent lateral hopping of adsorbed O atoms. A pressure exponent of $\beta = 0.7$ is explained by the similarity in

a)Author to whom correspondence should be addressed. Electronic mail: mlusk@mines.edu. Tel.: 303-273-3675. Fax: 303-273-3919.

barriers for two types of dissociation events: O_2 inserted into Si–Si backbonds that share the same Si–H bond; and, insertions into two separated Si–H bonds. These observations are consistent with a recent work[30] wherein similarly prepared H–Si(111) was exposed to an ambient atmosphere. Although the measurements were performed at a single temperature, $T = 293.15$ K, the prefactor of 10^{13}–10^{15} determined by Zhang *et al.*[29] can be used to estimate an effective oxidation barrier of 1.0–1.2 eV. The lower value, in comparison to Zhang *et al.* can be attributed to the oxidizing contributions of H_2O, NO_2, O_3, etc. from the ambient environment.

As an alternative to H passivation, alkyl groups are also widely used to terminate Si surfaces due to their flexibility, biocompatibility, and stability in a wide range of environments.[31] Densely packed, alkyl-terminated Si(001) and Si(111) surfaces are thermally stable up to 615 K.[32, 33] Bansal *et al.* reported that the in-air formation of an oxide monolayer with 50% coverage took 3 h, 5 h, and 2 days for the H−, CH_3^-, and long alkyl chain termination, respectively.[34] They concluded that exposure to O_2 simply results in oxidation of the organic ligands with very limited subsequent oxidation of the silicon substrate. Specifically, both multiple-internal-reflection infrared and x-ray photoelectron spectra showed that the number of C–O and O–C=O moieties increase with time, while the population of C=O first increases then slightly decreases with time. All of these bonds saturate after only a few hours, and the subsequent slow growth of C=O implies that it is formed by a sequence of two or more first-order reactions. The possible kinetics involves the sequential formation of intermediate molecular species, namely CH → C–O–O–H → C=O (or C–OH) → HO–C=O.[35, 36] The exact reaction sequence between O_2 and CH_3 ligand is not clear, though, and the corresponding activation energies remain unknown. These are issues that can be addressed using accurate quantum mechanical simulations.

First-principles investigations based on density functional theory (DFT) have been used to a surprisingly limited extent to quantify and elucidate the dissociative adsorption of O_2 on Si surfaces. For bare Si(001), a narrow, barrierless dissociation path was identified along which O_2 attacks dimer sites through chemisorption with intermediate states, and this was posited to be the dominant oxidation mechanism at room temperature.[37, 38] Computational queries of H-terminated Si surfaces have also been carried out,[22, 26, 39–43] and the results suggest that oxygen insertion into Si–Si bonds (Si–O–Si) is energetically more favorable than Si–O–H or Si=O insertions, consistent with experimental findings.[23, 25, 27] Early theoretical works also reported very high oxidation barriers for hydrogen terminated Si(111) surfaces. For instance, Teraishi *et al.*[43] suggested that the high effective barrier to oxidation was due to an activation energy of 2.2 eV for the formation of a precursor Si–O–O–Si structure that was predicted to subsequently decompose to create Si–O–Si bonds with only a tiny barrier. They also predicted that the oxidation barrier would be reduced for an Si atom that is already bonded to oxygen. However, their results are questionable because the reaction path assumed the existence of a Si–O–O–Si precursor, a structure that has never been observed experimentally. Furthermore, since

initial stage oxidation is a complicated dynamic process that almost certainly depends on O coverage, the effective barrier measured experimentally cannot be directly compared with the calculated barrier for a single O_2 adsorbed on the non-oxidized surface. The mobility of adsorbed O atoms was theoretically studied by Hoshino and Eyre[44, 45] who estimated the activation barriers for inward diffusion of an O atom on H–Si(111) and OH–(111) surfaces to be approximately 4 eV, much larger than that on the corresponding bare surface.

Modern first-principles transition state analysis provides the means to quantify precisely the role of terminating species in protecting Si surface from the earliest stages of oxidation. In the current work, dissociative adsorption pathways are identified for the first O_2 molecule adsorbed on H–Si(111), reconstructed H–Si(001), and unreconstructed H_2–Si(001), together with the subsequent mobility of O atoms. The role of hydrogen treatment in mitigating oxygen incorporation is made clear by computing the coverage dependence of the adsorption and hopping barriers for O as compared with bare surfaces. The initial oxidation of methyl-passivated surfaces is carefully considered as a representative of popular alkyl treatments. Dissociation on unreconstructed CH_3–Si(111) and reconstructed CH_3–Si(001) surfaces are analyzed, and barriers to the formation of key intermediate structures are used to corroborate and clarify experimentally motivated conjectures about the multi-step dissociation on alkyl-treated silicon.[35, 36]

II. COMPUTATIONAL METHODS AND MODELING

Our DFT calculations employed an all-electron approach with the exchange and correlation effects accounted for with the generalized gradient approximation formulated by Perdew, Burke, and Ernzerhof[46] and a real-space numerical atomic orbital basis.[47] A double numeric plus *d*-orbital basis was used, and structures were relaxed until the maximum atomic force is less than 0.1 eV/Å. Only the Γ point was needed for Brillouin zone sampling because of the large supercells involved.

Transition state (TS) searches were performed via the repeated, sequential application of linear synchronous transit and quadratic synchronous transit (QST) algorithms.[48] In each synchronous transit step, a series of total-energy calculations were performed on a set of interpolated structures, and the maximum energy structure along this path was used to generate an estimate for the transition state geometry. A conjugate gradient minimization followed by a QST analysis was repeated until the forces on all atoms were less than 0.27 eV/Å. This was followed by an eigenvector following (EF) analysis[49] in order to optimize the TS and its associated energy barrier. This was carried out using a Newton-like optimization algorithm applied to search for the energy maximum along a single (unstable) normal mode and the minimum along all other modes requiring a time-consuming diagonalization of the Hessian matrix. For both the TS search and EF analyses, a 0.028 eV electronic smearing was used. The procedure outlined is adaptive but in a perturbative way, requiring an initial guess for the pathway; therefore a large number of inequivalent pathways were considered as initial guesses for each of the processes considered in our investigation.

Calculations were performed using the $2\sqrt{2} \times 2\sqrt{2}$ H–Si(001) and 3×3 H–Si(111) supercells so that the distances between O in adjacent cells is approximately 10 Å, corresponding to roughly 10% oxygen coverage on the top surface. Each supercell contained eight layers because our calculations showed that the binding energy of O_2 molecules inserted on the center of the slab was well converged within 0.01 eV for 8 layers. The dangling bonds of the bottom layer were passivated with H atoms, and the bottom two layers of Si and H atoms were fixed during relaxations with a vacuum spacing of 40 Å. Due to steric effects, it is not possible to have 100% coverage of CH_3 ligands on the unreconstructed Si(001) surface so in this study only CH_3 passivated, reconstructed Si(001) surfaces were considered.

The binding energy is defined as $E_b = E$(Si surface) $+ E(O_2)$-E(Si surface with dissociated O_2). The activation barrier is likewise defined as $E_a = E$(TS)-E(initial state). These energies characterize the static and dynamic behavior of the system, respectively. Method accuracy was evaluated by calculating the barrier energies, E_a, for an O atom hopping from on-top to dimer, dimer to on-top, on-top to backbond, and backbond to on-top configurations on clean Si(001). The obtained values of 0.08, 1.12, 0.45, 1.45 eV, respectively, are very close to the corresponding values of 0.11, 1.11, 0.38, 1.34 eV reported previously using the nudged elastic band method with a plane wave basis set.[50] In addition, E_a for H_2 dissociation on reconstructed Si(001) was estimated to be 2.77 eV, which is in good agreement with the previously calculated value of 2.60 eV (Ref. [51]) and compares reasonably well with the experimental value of 2.22 ± 0.2 eV.[52]

III. RESULTS AND DISCUSSIONS

A. Dissociative adsorption of O_2 on H-terminated Si

It is well known that the oxidation rate on H-terminated Si is much lower than that of a corresponding bare surface.[53] The effective activation energies for initial stage oxidation on H–Si(111), H–Si(001), and H_2–Si(001) surfaces are estimated from experiments to be 1.7, 1.7, and 1.6 eV, respectively.[28, 29] It is tempting to make the interpretation that these barriers arise from O_2 dissociation and the subsequent breaking of Si–Si backbonds; however, our TS analysis indicates that there is *no barrier* for O_2 dissociation on either H–Si(111) or reconstructed H–Si(001) and that the barrier for unreconstructed H_2–Si(001) is only 0.05 eV. However, these barriers increase rapidly with increasing oxygen coverage, and steric effects cause this coverage sensitivity to be much greater for H–Si surfaces than for clean surfaces. Although a rapid diffusion of O atoms from the surface backbond sites might mitigate the effect of this coverage dependence, our results suggest that the barriers to both lateral and inward O hopping are significantly higher than those for clean surfaces.

1. O_2 adsorption on pristine surfaces

Four barrierless or nearly barrierless adsorption scenarios for the H–Si(111) surface were considered and are summarized in Fig. 1. The one with the lowest barrier and
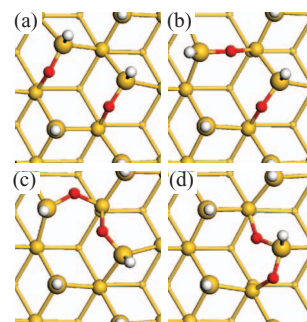

FIG. 1. Top view of four possible configurations for O_2 incorporation into H–Si(111) with associated barriers of 0.00, 0.00, 0.05, and 0.11 eV and binding energies of 8.14, 8.09, 7.65, and 7.79 eV in panels (a), (b), (c), and (d), respectively. Si atoms are tan, H atoms are white, and O atoms are red. The four different sizes of Si atom indicate the depth of the layer.

highest binding energy is shown in panel (a), where the two O atoms have the largest separation. In each case, the O_2 avoids H atoms as much as possible as it dissociates and hops to the backbond sites. The much higher activation energy $E_a = 2.2$ eV obtained in a previous theoretical study[43] is very likely due to an incorrectly prescribed reaction path which did not include the saddle point identified by the adaptive algorithm that we used. For instance, we found that a 0.3 Å displacement perpendicular to the imaginary frequency mode leads to an increase of 1.8 eV in the barrier height and suggests that the barrierless pathway is very narrow and easy to miss. If we change the path to form the intermediate structure Si–O–O–Si, then a 2.0 eV barrier is obtained, which is consistent to the previous calculation ($E_a = 2.2$ eV).[43] These additional results suggest that previous first-principle calculations failed to perform exhaustive searches of reaction paths.

It is also important to note that the activation energies for O_2 to be inserted into two Si–Si bonds sharing the same Si–H unit (Fig. 1(d)) and that with separated Si–H units (Figs. 1(a) and 1(c)) are similar, implying that both reactions contribute to the total oxidation rate. This is consistent with the explanation of Zhang *et al.* for a fitted pressure exponent of $\beta = 0.7$ in the reaction rate.[29]

In order to verify these rather surprising results, we exported the reaction path coordinates of thirty configurations associated with the reaction path of Fig. 1(a) and once again calculated the energy profile using a distinctly different DFT methodology. A plane-wave basis set with projected-augmented wave potentials[54] was implemented in the Vienna *ab-initio* simulations package (VASP) (Ref. [55]) with 480 eV energy cutoff. A comparison of the energy profiles, Fig. 2, shows essentially identical results with no barrier to oxygen dissociation. The small difference in final state energies (rightmost points) reduces to only 0.1 eV when the plane wave configuration is allowed to relax.

A consideration of H–Si(001) was then taken up with the final configurations for five possible paths to dissociative O_2 adsorption shown in Fig. 3. Two barrierless paths exist wherein two O atoms are inserted into neighboring dimer bonds (a) or backbonds in the same hexagonal cell (b). The much higher binding energy of (a) makes it the more probable scenario.
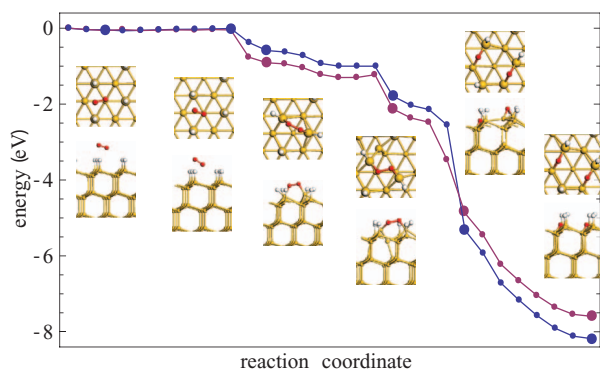
FIG. 2. Energy profile of the reaction path for O_2 adsorption on H–Si(111) corresponding to Fig. 1(a). Blue points were obtained from the original DFT TS analysis using an atomic orbital basis, while the red points are from energy calculations using identical geometries within a plane wave basis. Top view and side views of representative configurations are shown in the inset pictures with their associated positions in the energy profile denoted by larger dots.

Three possible oxidation paths were analyzed for the unreconstructed H_2–Si(001) surface, and their associated final configurations are shown in Fig. 4. In the lowest-E_a configuration (panel (a)), O atoms are adsorbed into neighboring Si–Si backbonds which share a first-layer Si atom. The activation energy for both scenarios (a) and (b) are slightly lower than those of corresponding paths on H–Si(001) (Figs. 3(c) and 3(e), respectively) because of the lower strain energy induced on H_2–Si(001). In contrast, the scenario in Fig. 4(c), where two O atoms are inserted into neighboring Si–Si backbonds sharing a second-layer Si atom, has a higher activation energy than the corresponding path on H–Si(001) (Fig. 3(b)). This is most likely because the expansion of the Si–Si backbonds on H_2–Si(001) reduces the distance between neighboring H dimers and thus increases their repulsion.

Three factors might affect the barrier of dissociative O adsorption on the H-terminated surfaces: steric repulsion between O_2 and nearby H atoms; bond distortion energy induced in the neighborhood of Si–Si bonds into which O atoms are insinuated; and steric repulsion between H atoms. The first two factors are believed to be more important, but the last factor might play a more substantial role on H_2–Si(001) surfaces, where the surface density of H is twice as high as on Si(111) and H–Si(001). Our TS simulations and Mulliken charge analyses suggest that O_2 gains negative charge as it approaches each of these surfaces. The additional charge occupies an anti-bonding orbital and causes the O=O bond to break, and the freed O atoms subsequently break Si–Si backbonds in a barrierless process.
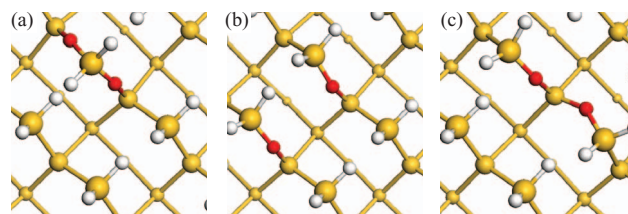
FIG. 4. Top view of three possible configurations for O_2 incorporation into unreconstructed H_2–Si(001) with associated barriers of 0.05, 0.09, and 0.22 eV and binding energies of 7.40, 7.55, and 7.40 eV in (a), (b), and (c), respectively.

2. Local O_2 coverage dependence

Adsorption of O_2 onto bare Si causes a local expansion of the Si lattice and compression elsewhere. This compression leads to stronger steric effects, requiring that subsequent adsorption events overcome a higher energy barrier. This is further exacerbated on H-terminated surfaces, where H atoms are pressed closer together with each O adsorption, and the trend is expected to be similar for H–Si(111) and H–Si(001), while that on H_2–Si(001) should be larger because of the higher H density on surface.

This coverage dependence was analyzed for H–Si(001) by calculating E_a for three configurations with a range of surface O content, and these are shown in Fig. 5. In scenario (a-to-d), a new dimer comes down on the periphery of a previously adsorbed O pair. The shorter distance between neighboring H atoms, decreased from 3.87 Å to 3.16 Å because of the first adsorption event, causes the energy barrier to increase from 0.0 eV to 0.63 eV. In the second scenario (b-to-e), a symmetric constraint is imposed on the adsorbing O dimer due to two previous absorption events. The distance between the two H atoms has been further reduced to 2.48 Å, causing the new adsorption barrier to increase to 1.21 eV. In the final scenario (c-to-f), two previous adsorption events result in four O atoms in an arrangement different than that of the (b-to-e) scenario. Here the barrier is slightly less, 0.44 eV. These results indicate that the O_2 adsorption barrier rises steeply with increasing O coverage, and that E_a is a function of not only O content but also local arrangement since (b-to-e) and (c-to-f) have the same O content. Such local coverage dependence turns out to have an immediate and strong influence on oxidation rates because of the low mobility of subsequent O hopping.

3. Oxygen diffusion

Our calculations of zero or very low barriers for the initial dissociative adsorption of oxygen are seemingly at odds with the effective barrier of 1.7 eV measured based on oxide layer
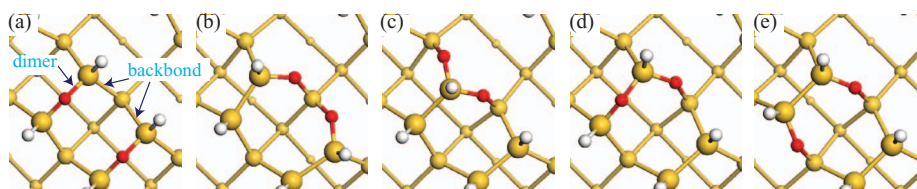

FIG. 3. Top view of five possible configurations for O_2 incorporation onto the reconstructed H–Si(001) with associated barriers of 0.00, 0.00, 0.13, 0.14, and 0.44 eV and binding energies of 8.16, 7.21, 7.38, 8.22, and 7.59 eV in panels (a), (b), (c), (d), and (e), respectively.
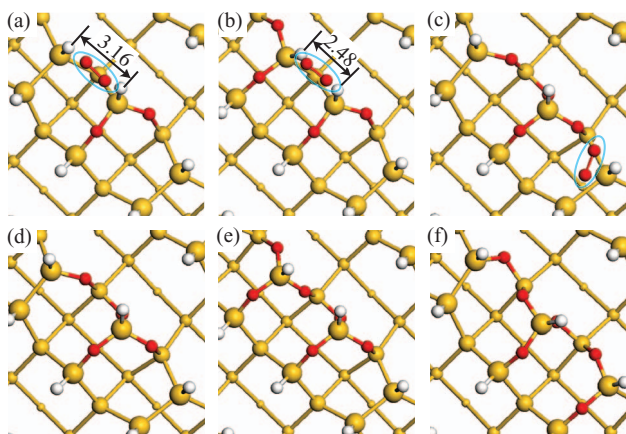
FIG. 5. Top views of initial (top row) and final (bottom row) configurations O_2 adsorption on partially oxidized H–Si(001) surfaces of varying O content. The associated barriers for scenario (a-to-d), (b-to-e), and (c-to-f) are 0.63, 1.24, and 0.44 eV, while the binding energies are 7.56, 8.08, and 7.87 eV, respectively. The detached O_2 molecule that is far away from the surface in the top panels is highlighted by blue ellipse in each initial configuration.

growth rates. Such measurements, though, implicitly account for what turns out to be very slow lateral diffusion of O atoms. This is consistent with the reaction order of 1.5, rather than 1, in density of Si–H obtained by fitting experiment data to the rate expression of Eq. (1),[29] implying a multistep oxidation process involving lateral hopping of O atoms.

We calculated E_a for three types of lateral O hops on H–Si(001), and the corresponding TS configurations are shown in Fig. 6. Oxygen hops from a backbond site to a: (a) neighboring dimer site; (b) backbond site lying on the neighboring hexagonal cell; and (c) neighboring backbond site in the same hexagonal cell. The hopping barriers were found to be 2.57, 2.61, and 2.78 eV, respectively. These values are much higher than analogous hopping barriers for *bare* Si(001) computationally estimated by Hemeryck *et al.*: 1.45, 1.72, and 2.43 eV.[56] The discrepancy is especially pronounced in the first two cases, in which the Si atom sitting on the middle of the path is fully passivated by a H atom, preventing the formation of an intermediate structure with an O atom attaching to the Si atom as occurs on clean surface. The pathways that we identified, though, are consistent with previous theoretical work which showed that, for negatively charged states, the barrier for lateral migration between neighboring backbond sites that share a second layer Si atom is much higher for H–Si(111) (1.8 eV) than for bare Si(111) (0.8 eV).[45] In the
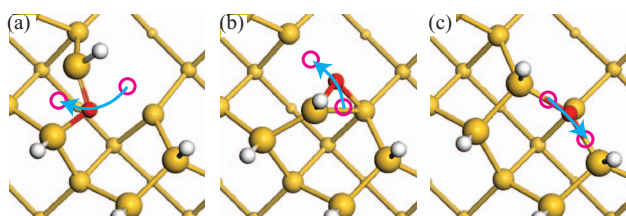

FIG. 6. Top view of TS configurations for lateral O hopping from one backbond to (a) neighboring dimer site, (b) backbond site in the neighboring hexagonal cell, and (c) backbond site in the same hexagonal cell on H–Si(001) surface. The red circles indicate the position of O for the initial and final structures, while the blue arrows highlight reaction pathways.
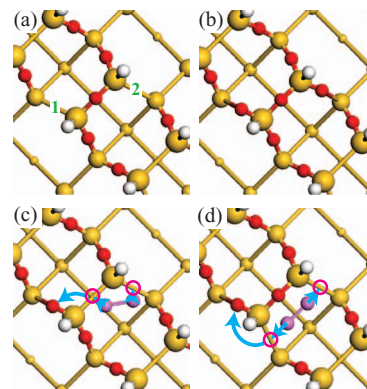

FIG. 7. Lateral diffusion of O atoms on H–Si(001) with subsequent dissociative adsorption of another O_2 molecule. Panel (a) shows the initial structure, while panel (b) shows the final structure with an new O_2 inserted into Si–Si bonds 1 and 2. Two possible intermediate structures are shown in panels (c) and (d), where the red circles denote the initial or final oxygen positions, and purple coloring is used to identify the newly arriving O_2.

third case, the lack of dangling bond on H–Si(001) makes it energetically less favorable to form an intermediate Si–O–Si bridge structure between two neighboring dimers so that the hopping barrier is consequently higher.

These high barriers to O hopping can have a strong influence on the rate of oxidation as illustrated in Fig. 7. There O atoms are dissociated into the Si substrate (panel a). Direct dissociative adsorption into sites 1 and 2 (panel b) is unlikely because the separation is too great, so a lateral O hop is required. Possible hops are shown in panels (c) and (d) for which the combined barriers for hop-plus-adsorption are 2.89 + 0.14 = 3.03 eV and 2.61 + 0.44 = 3.05 eV, respectively.

Our finding of the existence of barrierless oxidation path is consistent with the experimental measurements by Zhang *et al.*[29] Their effective oxidation barrier of 1.6 eV is composed of a coverage-dependent dissociation barrier and a subsequent O hopping barrier. As shown in Figs. 5(b) and 5(e), we found that the dissociation barrier of O_2 molecule could be as large as 1.24 eV in certain cases, and it is expected to be even higher as the O coverage increases. In addition, the calculated lateral hopping barrier of O atom on H–Si(111) surface is 2.48 eV. The combination of our calculated high lateral hopping barriers and O-coverage-dependent dissociation barriers explains the measured effective oxidation barrier of 1.6 eV.

In addition to the contribution from lateral hops, the slow rate of inward diffusion of O can also add to the stability against O_2 adsorption. Eyre *et al.*[45] estimated the inward hopping barrier for H–Si(111) to be 2.1 eV higher than that for a bare Si surface. They attributed the increase to the formation of a three-fold coordinated oxygen structure on clean Si(111) because of dangling bonds. H-terminated surfaces do not support such a three-fold structure, making diffusion more difficult. Our analysis of H–Si(111) gives an inward diffusion barrier of 2.82 eV, higher than the lateral diffusion barrier of 2.48 eV, indicating that the oxidation occurs as a layer-by-layer process on H–Si(111). In contrast, we estimate an inward diffusion barrier of 2.46 eV on H–Si(001), lower than the smallest lateral diffusion barrier of 2.61 eV. This is consistent with experimental observations that oxidation can happen both inside and on the surface for H–Si(001).[57,58]
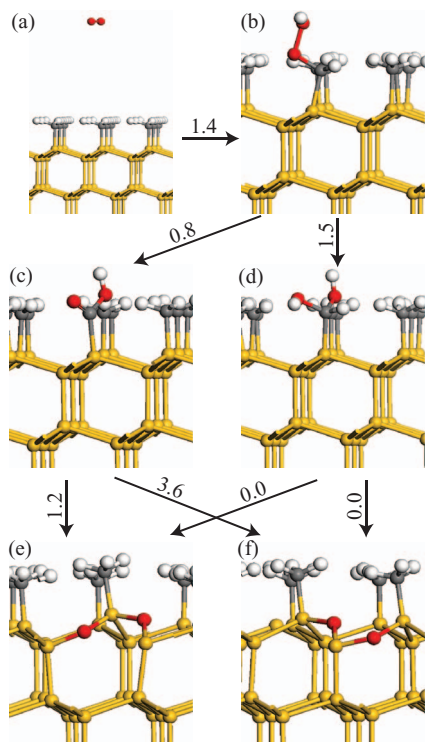
FIG. 8. Side view of possible reaction paths for O_2 adsorption on CH_3–Si(111) surface. Arrows indicate possible paths with associated activation energies given in eV.

B. O_2 adsorption on methyl-terminated Si

Alkyl-terminated Si surfaces offer much higher oxidation resistance than their H-terminated counterparts because of strong steric repulsion to O_2 (Ref. 35) that forces oxygen to chemically interact with the alkyl groups first, but the precise reactions steps have yet to be determined. Experimental work with long chain alkyls[36] suggests the following reaction sequence: CH → C–O–O–H → C=O (or C–OH) → HO–C=O. We have verified this computationally for methyl termination, and the analyses of Si(001) and Si(111) surfaces allow the intermediate structures to be elucidated and their barriers to be quantified.

1. Ligand oxidation

The reaction path for insertion of O_2 into a Si–Si backbond of CH_3–Si(111) contains three steps as illustrated in Fig. 8. O_2 approaching the surface (panel a) gains negative charge from the polarized CH_3 monolayer, generating an attraction between the O_2 and a positively charged H atom. This helps to break a C–H bond with a resulting intermediate structure C–O–O–H (panel b) which drops the energy by 1.41 eV after overcoming a barrier of 1.42 eV.

Oxygen atoms can then bond with the ligands in two ways, as shown in Fig. 8 panels (c) and (d). Both of these have been observed experimentally.[35,36] In the b → c transition, the O–O bond breaks, releasing a OH radical, then a H_2 molecule dissociates from CH_3 allowing the OH to dock in its place on the C atom. The resulting structure has one C=O double bond and one C–OH single bond with E_b = 2.32 eV and E_a = 0.80 eV. For the b → d path, the released
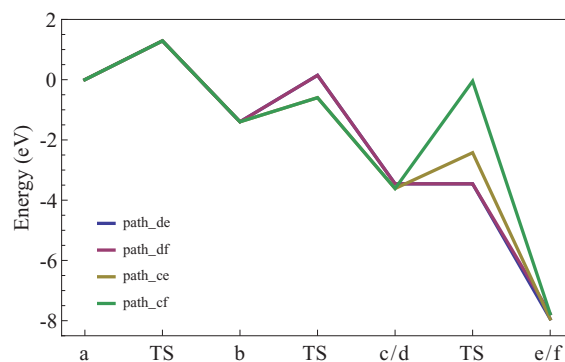

FIG. 9. Energy diagram of reaction paths for O_2 adsorption on CH_3–Si(111) shown in Fig. 8. The transition states are labeled with TS.

OH radical ruptures a C–H bond, and the released H atom then passivates the dangling bond of the remaining O atom on the ligand. This is followed by the recombination of the OH radical with C. The resulting structure has two C–OH bonds on the ligand with E_b = 2.06 eV and E_a = 1.54 eV.

Although the activation barrier for the b → c transition of Fig. 8 is lower than that for b → d, it is the latter structure that is favorable because of the subsequent steps in each case. O atoms hop from CH_3 to the Si–Si backbonds to form two Si–O–Si (siloxane) structures. This results in two inequivalent final states: configuration Fig. 8(e) with two O atoms connected to the same Si atom on the first layer; and Fig. 8(f) with two O atoms connected to a single Si atom on the second layer. The energy profiles of the four possible reaction paths, summarized in Fig. 9, indicate that a → b → d → e is the most
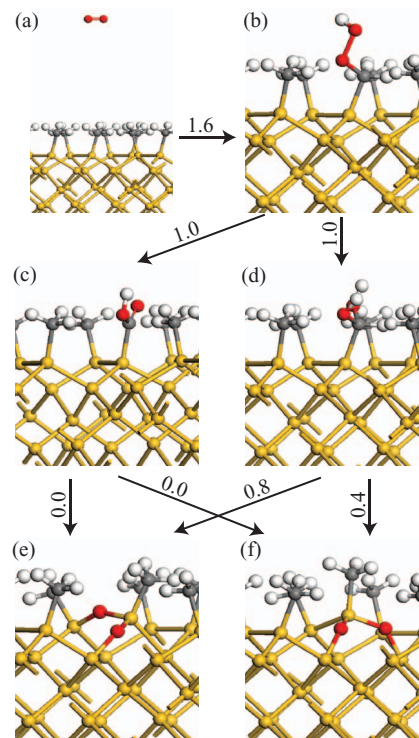

FIG. 10. Side view of possible reaction paths for O_2 adsorption on CH_3–Si(001) surface. Arrows indicate possible paths with associated activation energies given in eV.
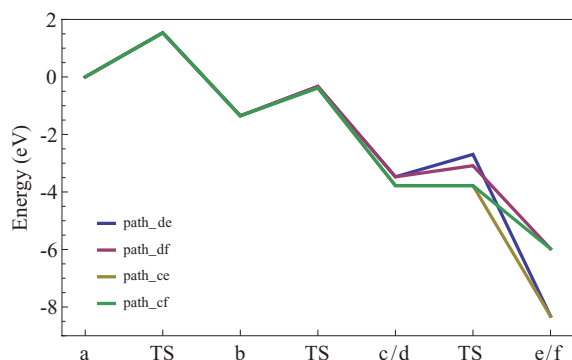
FIG. 11. Energy diagram of reaction paths for O_2 adsorption on CH_3–Si(001) shown in Fig. 10. The transition states are labeled with TS.

favorable reaction pathway since it has the lowest summed activation barrier total of 2.96 eV. This is consistent with the experimental observation of very slow initial state oxidation on methyl-terminated Si(111) surfaces.

2. Oxidation of CH_3–Si(001)

An analysis of methyl-terminated Si(001) identified an analogous three-step reaction path with comparable E_a as summarized in Fig. 10. The energy diagram is given in Fig. 11 with the a → b → c → e path having the lowest total barrier of 2.60 eV and the largest binding energy of 8.42 eV.

IV. SUMMARY

We have employed the density functional theory, combined with the transition-state analysis, to quantify the earliest steps for the oxidation of Si surfaces with two commonly used terminations. Hydrogen passivation forces oxygen to attack Si backbond sites, and a popular misunderstanding is that there is an activation barrier associated with the associated Si–Si bond breaking. Our results make clear that this is not the case; instead, there are many barrierless adsorption paths for the first incoming O_2 on H–Si(111) and H–Si(001), while the lowest activation energy on H_2–Si(001) surface is merely 0.05 eV. These adsorption barriers, however, increase remarkably as local O coverage is increased. If O could quickly hop inward or even laterally, this would not be as relevant to initial oxidation resistance, but the mobilities for both types of O diffusion on H-terminated surfaces are much lower than those of unpassivated surfaces. This is due to the lack of dangling bonds on H-terminated surfaces which prevent the formation of facilitating intermediate structures. This amplifies the effect of the surface content of O on further oxidation. Our results explain how H passivation, while offering essentially no barrier to initial oxygen attack, can still result in a slow rate of oxide growth corresponding to the experimentally measured 1.6 eV effective barrier associated with the formation of an oxide monolayer.

We have also quantified the precise mechanism by which oxidation begins on surfaces terminated with CH_3. Oxidation cannot proceed via direct dissociation into Si–Si bonds and follows a three-step process: adsorption of O_2 to form a

C–O–O–H intermediate structure; transition from C–O–O–H to C–O–H or C=O intermediates; and, hopping of an O atom from the ligand to the Si substrate. On both CH_3–Si(111) and CH_3–Si(001) surfaces, each of the first two steps has a barrier in the range of 0.8–1.5 eV, while the third step is barrierless. The lowest total activation barriers are 2.96 eV and 2.60 eV, respectively, for Si(111) and Si(001).

The approach used to analyze bulk Si is expected to be particularly profitable in the consideration of ways in which Si nanostructures can be protected from O attack. Even minuscule inroads of oxidation can have severe consequences for the optical and electronic performance of, for instance, assemblies of quantum dots and quantum wires, which are currently being investigated for their potential use in next-generation photovoltaic cells and light emission devices.

[1]M. Bohr, R. Chau, T. Ghani, and K. Mistry, IEEE Spectrum **44**, 29 (2007).
[2]A. V. Shah, J. Meier, E. Vallat-Sauvain, N. Wyrsch, U. Kroll, C. Droz, and U. Graf, Sol. Energy Mater. Sol. Cells **78**, 469 (2003).
[3]M. J. Kerr and A. Cuevas, Semicond. Sci. Technol. **17**, 35 (2002).
[4]E. Degoli and S. Ossicini, Surf. Sci. **470**, 32 (2000).
[5]J. Dalla Torre, J.-L. Bocquet, Y. Limoge, J.-P. Crocombette, E. Adam, G. Martin, T. Baron, P. Rivallin, and P. Mur, J. Appl. Phys. **92**, 1084 (2002).
[6]T. Yasuda, N. Kumagai, M. Nishizawa, S. Yamasaki, H. Oheda, and K. Yamabe, Phys. Rev. B **67**, 195338 (2003).
[7]H. Watanabe, K. Kato, T. Uda, K. Fujita, M. Ichikawa, T. Kawamura, and K. Terakura, Phys. Rev. Lett. **80**, 345 (1998).
[8]M. Shinohara, T. Katagiri, K. Iwatsuji, Y. Matsuda, H. Fujiyama, Y. Kimura, and M. Niwano, Thin Solid Films **475**, 128 (2005).
[9]K. Ohmori, H. Ikeda, H. Iwano, S. Zaima, and Y. Yasuda, Appl. Surf. Sci. **117**, 114 (1997).
[10]K. Inanaga, T. Nakahata, T. Furukawa, and K. Ono, Appl. Surf. Sci. **100**, 421 (1996).
[11]M. Ohashi and T. Hattori, Jpn. J. Appl. Phys., Part 2 **36**, L397 (1997).
[12]B. G. Yacobi, R. W. Collins, G. Moddel, P. Viktorovitch, and W. Paul, Phys. Rev. B **24**, 5907 (1981).
[13]G. Mauckner, K. Thonke, and R. Sauer, J. Phys.: Condens. Matter **5**, L9 (1993).
[14]T. Aiba, K. Yamauchi, Y. Shimizu, N. Tate, M. Katayama, and T. Hattori, Jpn. J. Appl. Phys., Part 1 **34**, 707 (1995).
[15]A. Kurokawa and S. Ichimura, Appl. Surf. Sci. **100**, 436 (1996).
[16]J. Westermann, H. Nienhaus, and W. Monch, Surf. Sci. **311**, 101 (1994).
[17]S. P. Garcia, H. Bao, M. Manimaran, and M. A. Hines, J. Phys. Chem. B **106**, 8258 (2002).
[18]Z. J. Cui and C. G. Takoudis, J. Electrochem. Soc. **150**, G694 (2003).
[19]M. Niwano, J. Kageyama, K. Kinashi, N. Miyamoto, and K. Honma, J. Vac. Sci. Technol. A **12**, 465 (1994).
[20]D. Kovalev, V. Y. Timoshenko, N. Künzner, E. Gross, and F. Koch, Phys. Rev. Lett. **87**, 068301 (2001).
[21]R. R. Koropecki, R. D. Arce, and J. A. Schmidt, Phys. Rev. B **69**, 205317 (2004).
[22]Y. J. Chabal, K. Raghavachari, X. Zhang, and E. Garfunkel, Phys. Rev. B **66**, 161315 (2002).
[23]H. Ikeda, Y. Nakagawa, M. Toshima, S. Furuta, S. Zaima, and Y. Yasuda, Appl. Surf Sci. **117**, 109 (1997).

[24]H. Ikeda, K. Hotta, S. Furuta, S. Zaima, and Y. Yasuda, Appl. Surf. Sci. **104**, 354 (1996).

[25]K. Sato, Y. Nakagawa, H. Ikeda, S. Zaima, and Y. Yasuda, Thin Solid Films **369**, 277 (2000).

[26]H. Kageshima, K. Shiraishi, H. Ikeda, S. Zaima, and Y. Yasuda, Appl. Surf. Sci. **159**, 14 (2000).

[27]X. D. Pi, L. Mangolini, S. A. Campbell, and U. Kortshagen, Phys. Rev. B **75**, 085423 (2007).

[28]X. Zhang, Y. J. Chabal, S. B. Christman, E. E. Chaban, and E. Garfunkel, J. Vac. Sci. Technol. A **19**, 1725 (2001).

[29]X. Zhang, E. Garfunkel, Y. J. Chabal, S. B. Christman, and E. E. Chaban, Appl. Phys. Lett. **79**, 4051 (2001).

[30]M. Kolibal, J. Cechal, M. Bartosik, J. Mach, and T. Sikola, Appl. Surf. Sci. **256**, 3423 (2010).

[31]S. F. Bent, J. Phys. Chem. B **106**, 2830 (2002).

[32]M. M. Sung, G. J. Kluth, O. W. Yauw, and R. Maboudian, Langmuir **13**, 6164 (1997).

[33]R. Hunger, R. Fritsche, B. Jaeckel, W. Jaegermann, L. J. Webb, and N. S. Lewis, Phys. Rev. B **72**, 045317 (2005).

[34]A. Bansal, X. Li, I. Lauermann, N. S. Lewis, S. I. Yi, and W. H. Weinberg, J. Am. Chem. Soc. **118**, 7225 (1996).

[35]L. J. Webb, D. J. Michalak, J. S. Biteen, B. S. Brunschwig, A. S. Y. Chan, D. W. Knapp, H. M. Meyer, E. J. Nemanick, M. C. Traub, and N. S. Lewis, J. Phys. Chem. B **110**, 23450 (2006).

[36]D. Aureau, W. Morscheidt, A. Etcheberry, J. Vigneron, F. Ozanam, P. Allongue, and J.-N. Chazalviel, J. Phys. Chem. C **113**, 14418 (2009).

[37]K. Kato, T. Uda, and K. Terakura, Phys. Rev. Lett. **80**, 2000 (1998).

[38]X. L. Fan, Y. F. Zhang, W. M. Lau, and Z. F. Liu, Phys. Rev. Lett. **94**, 016101 (2005).

[39]M. Halls and K. Raghavachari, J. Phys. Chem. B **108**, 19388 (2004).

[40]X.-Y. Deng, C. Yang, M.-X. Zhou, W.-F. Yuc, and J.-S. Li, Chin. J. Chem. Phys. **19**, 485 (2006).

[41]K. Teraishi, H. Takaba, A. Yamada, A. Endou, I. Gunji, A. Chatterjee, M. Kubo, A. Miyamoto, K. Nakamura, and M. Kitajima, J. Chem. Phys. **109**, 1495 (1998).

[42]K. Sakata, T. Sato, K. Nakamura, A. Osamura, and A. Tachibana, Appl. Surf. Sci. **159–160**, 392 (2000).

[43]K. Teraishi, A. Endou, I. Gunji, M. Kubo, A. Miyamoto, and M. Kitajima, Surf. Sci. **426**, 290 (1999).

[44]T. Hoshino and Y. Nishioka, Phys. Rev. B **64**, 125322 (2001).

[45]R. J. Eyre, J. P. Goss, and P. R. Briddon, Phys. Rev. B **76**, 245325 (2007).

[46]J. P. Perdew and Y. Wang, Phys. Rev. B **45**, 13244 (1992).

[47]B. Delley, J. Chem. Phys. **92**, 508 (1990).

[48]T. A. Halgren and W. N. Lipscomb, Chem. Phys. Lett. **49**, 225 (1977).

[49]J. C. Mauro, R. J. Loucks, and J. Balakrishnan, J. Phys. Chem. A **109**, 9578 (2005).

[50]A. Hemeryck, A. J. Mayne, N. Richard, A. Esteve, Y. J. Chabal, M. D. Rouhani, G. Dujardin, and G. Comtet, J. Chem. Phys. **126**, 114707 (2007).

[51]G. Li, Y.-C. Chang, R. Tsu, and J. E. Greene, Surf. Sci. **330**, 20 (1995).

[52]D.-S. Lin and R.-P. Chen, Phys. Rev. B **60**, R8461 (1999).

[53]G. Higashi, Y. Chabal, G. Trucks, and K. Raghavachari, Appl. Phys. Lett. **56**, 656 (1990).

[54]P. E. Blöchl, Phys. Rev. B **50**, 17953 (1994).

[55]G. Kresse and J. Furthmüller, Comput. Mater. Sci. **6**, 15 (1996).

[56]A. Hmeryck, A. Estve, N. Richard, M. D. Rouhani, and G. Landa, Surf. Sci. **603**, 2132 (2009).

[57]G. J. Kluth and R. Maboudian, J. Appl. Phys. **80**, 5408 (1996).

[58]Y. Narita, F. Hirose, M. Nagato, and Y. Kinoshita, Thin Solid Films **517**, 209 (2008).